Available online at www.sciencedirect.com
ScienceDirect
Journal of Sound and Vibration 323 (2009) 51–66
JOURNAL OF SOUND AND VIBRATION
www.elsevier.com/locate/jsvi

Increase in transmission loss of a double panel system by addition of mass inclusions to a poro-elastic layer: A comparison between theory and experiment

Kamal Idrisi[a,*], Marty E. Johnson[a], Alessandro Toso[a], James P. Carneal[b]

[a] *Vibration and Acoustics Labs,136 Durham Hall, Virginia Tech, 24061, USA*
[b] *GE Energy, 3901 Castle Hayne Road, Wilmington, NC 28401, USA*

Received 5 March 2008; received in revised form 3 December 2008; accepted 9 December 2008
Handling Editor: S. Bolton
Available online 7 February 2009

Abstract

This paper is concerned with the modeling and optimization of heterogeneous (HG) blankets, which are used in this investigation to reduce the sound transmission through double panel systems. HG blankets consist of poro-elastic media with small embedded masses, which act similarly to a distributed mass–spring–damper-system. HG blankets have shown significant potential to reduce low frequency radiated sound from structures, where traditional poro-elastic materials have little effect. A mathematical model of a double panel system with an acoustic cavity and HG blanket was developed using impedance and mobility methods. The predicted responses of the source and the receiving panel due to a point force are validated with experimental measurements. The presented results indicate that proper tuning of the HG blankets can result in broadband noise reduction below 500 Hz with less than 10% added mass.

1. Introduction

This paper presents part of the work that has been done to develop a new passive noise control device that is used to reduce aircraft interior noise across a broad frequency spectrum. Significant progress has been made in the last five decades in the understanding, the prediction, and the control of interior aircraft noise [1]. There are several methods to reduce the interior noise levels, including source reduction, active [2,3] and passive control of the aircraft transmission paths, and active control of the sound field [4,5].

Active methods have been extensively studied and have been applied in practice in propeller driven aircraft, [6,7] but use is limited as passive control methods are less expensive, less complicated, and do not require any control energy.

Passive treatments used in civil aircraft can be broadly grouped into damping materials and acoustic absorbers. Acoustic barriers are too heavy for aircraft application. The common trait of passive treatments is

*Corresponding author. Tel.: +1 540 231 4162.
E-mail addresses: idrisi@vt.edu (K. Idrisi), martyj@vt.edu (M.E. Johnson), aletoso@vt.edu (A. Toso), jcarneal@yahoo.com (J.P. Carneal).

0022-460X/$ - see front matter © 2009 Elsevier Ltd. All rights reserved.
doi:10.1016/j.jsv.2008.12.026

that they work well at high frequencies [8,9], while low-frequency, passive control requires heavy installations. Damping material with different configurations can be mounted on the fuselage skin [10] as well as to frames, stringers, [11] and the trim panels [12]. Parts of the damping material often consist of visco-elastic material which dissipates energy in addition to adding stiffness. However, it is also known to have a limited operating temperature range. Although the damping of visco-elastomers is high, the stiffness of the material changes rapidly with temperature caused by both external conditions and internal heating due to energy dissipation.

Acoustic damping materials such as fiberglass or polyamide reduce the sound in enclosures by converting the mechanical motion of the air particles into low-level heat. These acoustic blankets are limited in their performance at low frequency by the thickness of the fuselage wall cavity as their effectiveness in controlling low-frequency noise increases with material thickness. They are only effective at frequencies above about 500 Hz [13].

One method to control low-frequency transmissions uses damped resonant devices such as Helmholtz resonators, dynamic vibration absorbers, and tuned vibration dampers. These have been shown to provide significant reduction at low frequencies while limiting the added mass to 10% of the untreated structure [14]. However, these are devices that must be used in addition to the traditional passive treatments used for broadband-noise control.

From the above analysis, it is evident that an integrated passive solution that can control noise transmission across the entire bandwidth is needed. One resonant device developed and tested for broadband control in the last decade is the distributive vibration absorber which consists of a plate bonded to sound absorbing foam. The resonance of the distributive vibration absorber can be tuned by varying the loading mass, or the effective stiffness of the acoustic foam. The distributive vibration absorbers were tested on a rotorcraft fuselage. The distributive vibration absorbers were mounted on top of cut-outs of the standard layer of porous media inside the fuselage shell. Experimental results have shown that the distributive vibration absorbers were very effective at reducing the vibration response at targeted resonant spikes at low frequencies [15]. Once this technology was proven, the natural progression was to insert the masses inside the porous media instead of mounting the distributive vibration absorber on top of the porous layer. In this way, the stiffness of the poro-elastic material was used as spring elements of the distributive vibration absorber. This leads to the development of a new passive control treatment for sound transmission through base structures, called a heterogeneous (HG) blanket.

HG blankets combine two passive control mechanisms (damping and dynamic absorption) into a single control treatment that has the potential to control a wide frequency range. The HG blanket consists of poro-elastic media such as acoustic foam with small embedded masses, which act similarly to a distributed mass-spring-damper system as seen in a schematic presented in Fig. 1(a). Recent experimental investigations carried out by Kidner et al. [16] as well as numerical and experimental studies conducted by Sgard et al. [17,18] showed that HG blankets have significant potential to reduce low-frequency, radiated sound from structures;

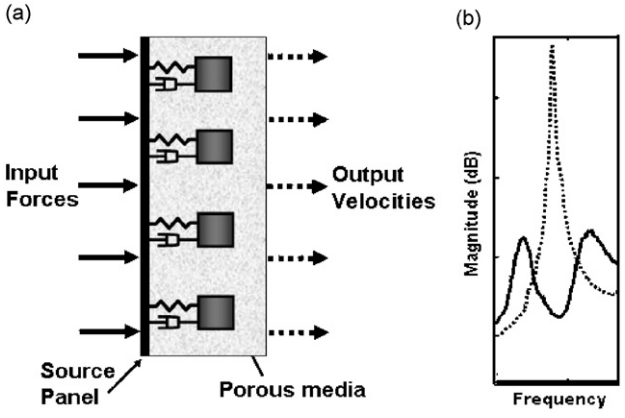

Fig. 1. Schematic of plate with HG blanket mounted on top (a) and schematic of damped mode split effect of the HG blanket, before (------) and after (——) targeting base structure mode (b).

traditional poro-elastic materials have little effect [8,9]. This can be accomplished without losing the good performance at high frequencies due to the presence of porous media. Kidner also came to the conclusion that HG blankets can be more efficient when the embedded masses are positioned to target certain modes instead of randomly distributing the masses. In order to target a plate mode, it is necessary to "tune" the embedded mass to the desired frequency as well as position it at certain anti-node lines of the mode. "Tuning" the mass insertions can be achieved by varying the depth of the mass position inside the poro-elastic media or by varying the weight and mass shape of the embedded mass [19]. Proper "tuning" of the masses will result into a mode split of the targeted resonance of the base structure. Following traditional tuned-vibration absorber theory [20], the targeted resonance peak is then split into two resultant peaks, one above and one below the original peak. If the damping ratio is correctly designed [21,22], both resultant resonant frequencies have lower and more damped amplitudes than the original resonance as shown schematically in Fig. 1(b). Note that one can minimize the two "resultant" peaks by optimizing the damping level.

The objective here is to investigate the use of HG blankets for the control of sound transmission through double-panel systems, and specifically this paper presents the explicit coupling equations used to predict the response of a double-panel system with sandwiched HG blanket and air cavity. An impedance and mobility method approach is used to couple the analytical models of the air cavity, the source (fuselage), and the receiving (trim) panels with a finite element model of the HG blanket. An assembled matrix approach is developed that allows a straightforward expansion of the model and solves for all velocities and forces at the interfaces. The mathematical model of the double-panel system is experimentally validated with and without the HG blanket. The responses of the fuselage and trim panel are plotted in terms of spatially averaged squared velocity as well as the total acoustic power radiated from the double-panel system.

2. Mathematical model

This section presents the mathematical model used to predict the sound radiation and vibration response of a double panel system with sandwiched HG blanket. The system investigated consists of 5 components: the fuselage panel or fuselage, HG blanket, air cavity, the trim panel or trim, and the acoustic free field, which are all shown in Fig. 2.

The fuselage and trim were both modeled as flat plates [23], where the plate modes from Warburton [24] were used. The foam is modeled using poro-elastic finite elements based on fundamental fluid, structural, and coupled fluid-structural equations given by Panneton and Atalla [17,18,25]. A mesh of 8-node brick elements has been used. The HG blanket itself was developed adding point masses to the poro-elastic mass matrix. The air cavity is modeled using the modes for a rectangular rigid wall volume, and the modes are given by Kinsler and Frey [26]. The radiation into the acoustic free field is modeled as per Elliott and Johnson [27] using an elemental radiator approach. Note that the diagonal terms lead to a singularity, but the problem can be avoided as per Bai and Tsao [28] by changing the domain from rectangular to circular in the Rayleigh formula, or as per Berkhoff [29] using the boundary element method.

To combine the individual models into a system, the forces and velocities at the interfaces need to be equated. This can be achieved most effectively using the impedance and mobility method, which couples the components together at discretized locations on the interfaces. The impedance and mobility method was originally proposed by Firestone [30] and further developed by Gardonio and Brennan [31,32].

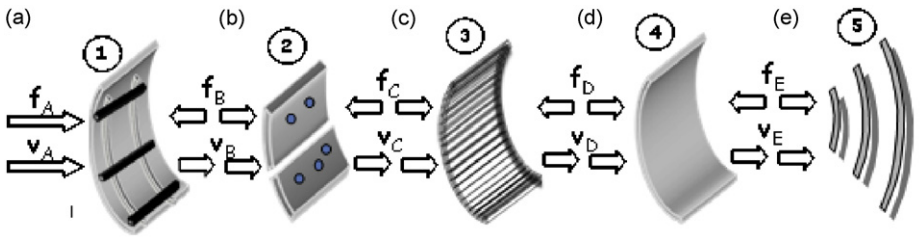

Fig. 2. Objects incorporated in mathematical model of the double panel system: Fuselage (1), HG blanket (2), air cavity (3), trim (4) and interior acoustic field (5). Interfaces between objects are noted with capital letters A–E.

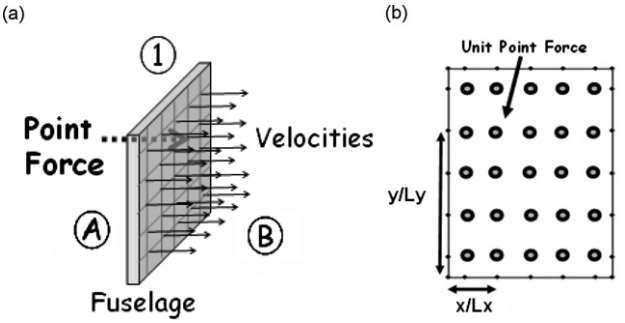

Fig. 3. Schematic of: (a) point force acting off center on a fuselage with 25 output velocities at grid nodes and (b) the mesh of 5×5 nodes used to compare theory and experiment for the double panel system along with the position of the unit point force excitation.

For this work, all subsystems were discretized using a 5×5 grid as shown in Fig. 3. For a given component, at each frequency, a mobility matrix can be formed that describes the relationship between all output velocities and all forces in a 25×25 matrix. The matrices describing the behavior of each component are calculated by the aforementioned analytical and finite element models. The detailed derivation of these matrices is beyond the scope of this paper, and can be found in the references. These matrices can then be assembled into a larger system matrix, which is described in detail later.

For this derivation, the low frequency assumption is used, i.e. the subsystems of the double panel system are assumed to be moving with transverse motion only, therefore moments and axial forces are neglected. Both, the fuselage as well as the trim panel have clamped boundary conditions. In addition, it should be noted that the panels of a civil aircraft fuselage are curved and coupled through mounts while the numerical model in this work assumes flat panels and coupling of the fuselage and trim panel through the air cavity. This is a common assumption widely used in literature [3,33].

2.1. System studied

The double panel system studied consists of a fuselage and a trim panel. The fuselage panel, referred to as the "fuselage", can be excited by a point force. For the work presented here a unit force acting at $x/L_x = 0.3$ and $y/L_y = 0.7$ on the fuselage panel is used.

Fig. 2 shows the system studied in the mathematical model. The modeled objects are labeled 1–5, which are the fuselage, HG blanket, cavity, trim and radiation field, respectively. The interfaces of this subsystem are labeled A–E which are the input force/fuselage, fuselage/HG blanket, HG blanket/cavity, cavity/trim and trim/radiation field interfaces, respectively.

2.2. Explicit coupling equations for the system

To couple the objects, a linear system of equations was derived using the continuity of velocity and equilibrium of forces at all interfaces A → E. Mobility and impedance representations for each object 1 → 5 were derived. The impedance and mobility matrices have three indexes. The first index stands for the object number. The second index points out the interface at which the forces on the objects act. The third index shows at which interface the velocities are computed. For example, at a given frequency, the complex mobility matrix $\mathbf{M}_{1AB}$ would describe the velocities at interface B due to forces acting on interface A acting through the first object (1). Hence, $\mathbf{M}_{1AB}$ is a transfer mobility matrix with the input force described by the complex vector $\mathbf{f}_A$ and output velocities described by a complex vector $\mathbf{v}_B$. Fig. 3 shows a schematic of the fuselage with the input point force off center and the 25 output velocities that describe one column of the mobility matrix $\mathbf{M}_{1AB}$. The impedance matrices $\mathbf{Z}$ are indexed analog to the mobility matrices. The coupling equations for interface B are:

$$\mathbf{v}_B = \mathbf{M}_{1AB}\mathbf{f}_A - \mathbf{M}_{1BB}\mathbf{f}_B, \tag{1}$$

$$\mathbf{f}_B = \mathbf{Z}_{2BB}\mathbf{v}_B + \mathbf{Z}_{2BC}\mathbf{v}_C. \tag{2}$$

$\mathbf{M}_{1BB}$ and $\mathbf{f}_B$ are the mobility of the fuselage [23] (modeled using analytical plate equations) and the force acting at the interface B, respectively. $\mathbf{Z}_{2BB}$ and $\mathbf{Z}_{2BC}$ (see Appendix A) are derived from the finite element model for the HG blanket. The equations for interface C are:

$$\mathbf{f}_C = -\mathbf{Z}_{2CB}\mathbf{v}_B - \mathbf{Z}_{2CC}\mathbf{v}_C, \tag{3}$$

$$\mathbf{f}_C = \mathbf{Z}_{3CC}\mathbf{v}_C - \mathbf{Z}_{3CD}\mathbf{v}_D. \tag{4}$$

$\mathbf{Z}_{2CB}$ and $\mathbf{Z}_{2CC}$ (see Appendix A) are also calculated from the finite element model. $\mathbf{Z}_{3CC}$ and $\mathbf{Z}_{3CD}$ [26] (calculated using the modes for a rectangular rigid wall volume) are the input and transfer impedance of the cavity, respectively. The equations for interface D are as follows:

$$\mathbf{f}_D = \mathbf{Z}_{3DC}\mathbf{v}_C - \mathbf{Z}_{3DD}\mathbf{v}_D, \tag{5}$$

$$\mathbf{v}_D = \mathbf{M}_{4DD}\mathbf{f}_D - \mathbf{M}_{4ED}\mathbf{f}_E, \tag{6}$$

with $\mathbf{Z}_{3DC}$ and $\mathbf{Z}_{3DD}$ [26] being the cavity transfer and output impedance, respectively. The coupling equations for the last interface, E, are

$$\mathbf{v}_E = \mathbf{M}_{4DE}\mathbf{f}_D - \mathbf{M}_{4EE}\mathbf{f}_E, \tag{7}$$

$$\mathbf{f}_E = \mathbf{Z}_{5EE}\mathbf{v}_E. \tag{8}$$

where the mobility matrices of the trim are $\mathbf{M}_{4DD}$, $\mathbf{M}_{4DE}$, $\mathbf{M}_{4ED}$, and $\mathbf{M}_{4EE}$. (calculated similar to the fuselage mobility matrices) The velocity at the trim surface is then multiplied by the radiation impedance matrix $\mathbf{Z}_{5EE}$ (Eq. (8)) as per Elliott et al., Bai et al. and Berkhoff [27–29] (derived using boundary element method or Rayleigh integral formula in the case of planar sources in a baffle) to account for radiation loading $\mathbf{f}_E$. It should be noted that in practice, accelerometers were used to measure the fuselage and trim response. In order to match theory with experiment, these accelerometers were modeled as lumped masses placed on the plates at the nodes at which the accelerometers were positioned. The derivation of the explicit coupling matrices makes it possible to solve for the velocities and forces at the interfaces of interests.

2.3. Assembled matrix representation

There are several potential methods to solve the above set of coupled equations, from direct algebraic manipulation to a matrix method. Solving for each variable individually by manipulating Eqs. (1)–(8) is a tedious process and prone to mathematical errors, so it was decided to write the linear set of coupled equations as an assembled matrix:

$$\underbrace{\begin{bmatrix} \mathbf{M}_{1BB} & \mathbf{I} & \mathbf{0} & \mathbf{0} & \mathbf{0} & \mathbf{0} & \mathbf{0} & \mathbf{0} \\ \mathbf{I} & -\mathbf{Z}_{2BB} & \mathbf{0} & -\mathbf{Z}_{2BC} & \mathbf{0} & \mathbf{0} & \mathbf{0} & \mathbf{0} \\ \mathbf{0} & \mathbf{Z}_{2CB} & \mathbf{I} & \mathbf{Z}_{2CC} & \mathbf{0} & \mathbf{0} & \mathbf{0} & \mathbf{0} \\ \mathbf{0} & \mathbf{0} & \mathbf{I} & -\mathbf{Z}_{3CC} & \mathbf{Z}_{3CD} & \mathbf{0} & \mathbf{0} & \mathbf{0} \\ \mathbf{0} & \mathbf{0} & \mathbf{0} & -\mathbf{Z}_{3DC} & \mathbf{Z}_{3DD} & \mathbf{I} & \mathbf{0} & \mathbf{0} \\ \mathbf{0} & \mathbf{0} & \mathbf{0} & \mathbf{0} & \mathbf{I} & -\mathbf{M}_{4DD} & \mathbf{M}_{4ED} & \mathbf{0} \\ \mathbf{0} & \mathbf{0} & \mathbf{0} & \mathbf{0} & \mathbf{0} & -\mathbf{M}_{4DE} & \mathbf{M}_{4EE} & \mathbf{I} \\ \mathbf{0} & \mathbf{0} & \mathbf{0} & \mathbf{0} & \mathbf{0} & \mathbf{0} & \mathbf{I} & -\mathbf{Z}_{5EE} \end{bmatrix}}_{\mathbf{A}} \underbrace{\begin{bmatrix} \mathbf{f}_B \\ \mathbf{v}_B \\ \mathbf{f}_C \\ \mathbf{v}_C \\ \mathbf{v}_D \\ \mathbf{f}_D \\ \mathbf{f}_E \\ \mathbf{v}_E \end{bmatrix}}_{\mathbf{x}} = \underbrace{\begin{bmatrix} \mathbf{M}_{1AB}\mathbf{f}_A \\ \mathbf{0} \\ \mathbf{0} \\ \mathbf{0} \\ \mathbf{0} \\ \mathbf{0} \\ \mathbf{0} \\ \mathbf{0} \end{bmatrix}}_{\mathbf{b}}, \tag{9}$$

which can then be solved by inverting the matrix $\mathbf{A}$ as well as iteratively. *Matrix* $\mathbf{A}$ is a sparse and almost block diagonal matrix and therefore efficiently invertible [34] as. Taking a closer look at $\mathbf{A}$, one can recognize that it consists of small sub matrices such as

$$\begin{bmatrix} -\mathbf{Z}_{3CC} & \mathbf{Z}_{3CD} \\ -\mathbf{Z}_{3DC} & \mathbf{Z}_{3DD} \end{bmatrix}, \tag{10}$$

which represent the cavity in the observed case. This shows that it is very easy to add more levels of complexity to an existing system using the matrix formulation, without needing to use algebraic manipulation.

3. Comparison between theory and experimental results

This section presents the experimental validation of a double panel system with and without the HG blanket. Fig. 4(a) shows the schematic of the experimental setup with the two clamps (1,6) supporting the clamped boundary conditions of the fuselage (2) and the trim (5). The HG blanket (3) is attached to the "interior" of the fuselage. A heavy aluminum block was used as the frame (4). Pictures of the experimental setup in Fig. 4(b) show the accelerometer position, grid (left) and the frame (right). A roving modal hammer excited the fuselage at all of the grid points, and transfer functions from the hammer to accelerometer were measured. Using reciprocity, these can be viewed as a roving accelerometer and a constant position point force excitation, which match the model.

Throughout the paper, *the spatially averaged squared velocity* of the fuselage V_f and trim V_t are used to present the predicted response of the double panel system. At each frequency of interest, V_f and V_t are calculated from 25 by 1 complex vectors of fuselage and trim velocities $\mathbf{v}_f$ and $\mathbf{v}_t$:

$$V_f = \frac{1}{N}\mathbf{v}_f^{\mathbf{H}}\mathbf{v}_f,$$

$$V_t = \frac{1}{N}\mathbf{v}_t^{\mathbf{H}}\mathbf{v}_t \tag{11}$$

These measures are directly proportional to the kinetic energy of the plates as per Gardonio and Elliott [3]. Furthermore the *total sound power* radiated from the double panel system with sandwiched HG blanket can be expressed as follows:

$$P_t = \frac{1}{N}\mathbf{v}_t^{\mathbf{H}}\mathbf{Z}_{5EE}\mathbf{v}_t, \tag{12}$$

where $\mathbf{Z}_{5EE}$ is the radiation matrix used in Eq. (8) as per Elliott et al., Bai et al. and Berkhoff [27–29]. These calculations can then be performed over the frequencies range of interest (0–500 Hz).

3.1. Experimental validation for double panel system

This section presents the results of the experimental validation of the coupled double panel system without the HG blanket. Table 1 lists all important properties of the double panel system with two clamped plates used for the experimental validation of the analytical model. To match the experimental fuselage and trim panel in the analytical model, the aspect ratio has been changed on both plates within 2–3% of the measured values, and the damping ratio for all modes has been set to 0.006, which is typical for a clamped aluminum plate.

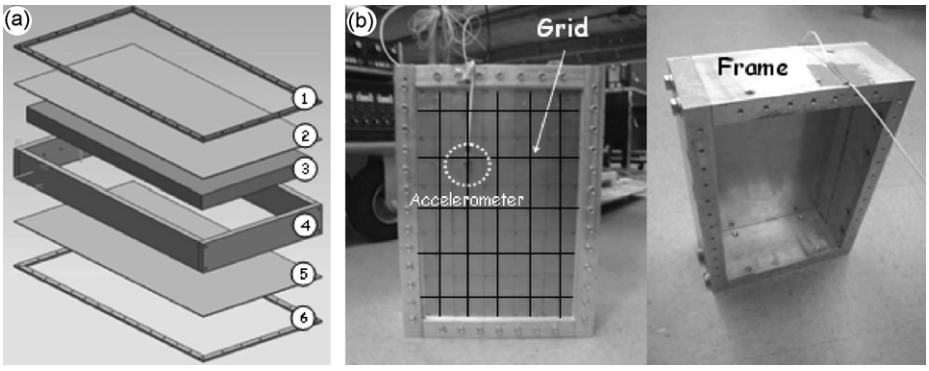

Fig. 4. Experimental setup: schematic (a) and pictures (b) showing the accelerometer position and 5×5 grid (left) as well as the frame (right).

Fig. 5(a) shows the experimental validation of the double panel system on the fuselage side, excited at $x/L_x = 0.1$ and $y/L_y = 0.7$ as shown in Fig. 3. Theory and experiment match very well and the dynamics of the fuselage are all captured with a high level of detail. Most of the discrepancies can be explained by slight differences in damping level between experiment and theory. For simplicity, the analytical model uses a constant damping term for all of the modes and the damping was not changed from mode to mode. This can be particularly seen at the third mode, around 200 Hz, which is much lower in the measured spectrum than in the model. However, the third experimental mode is an even–odd mode (2–1) [35] which does not couple very well to the cavity and thus is not very important for sound transmission.

Fig. 5(b) presents the experimental validation of the double panel system on the receiving side, measured at 25 points with the fuselage panel excited at acting at $x/L_x = 0.1$ and $y/L_y = 0.7$ as shown in Fig. 3.

Table 1
Model parameters of the double panel system with two clamped plates.

Parameter	Value	Units
Material properties of the fuselage		
Length	0.307	m
Width	0.206	m
Thickness	0.0008	m
Density	2700	kg/m^3
Modulus of elasticity	7×10^{10}	N/m^2
Poisson's ratio	0.3	–
Material properties of the cavity		
Thickness	0.1	m
Density	1.2	kg/m^3
Speed of sound	343	m/s
Damping	0.01	–
Material properties of the trim		
Length	0.307	m
Width	0.206	m
Thickness	0.0012	m
Density	2700	kg/m^3
Modulus of elasticity	7×10^{10}	N/m^2
Poisson's ratio	0.3	–

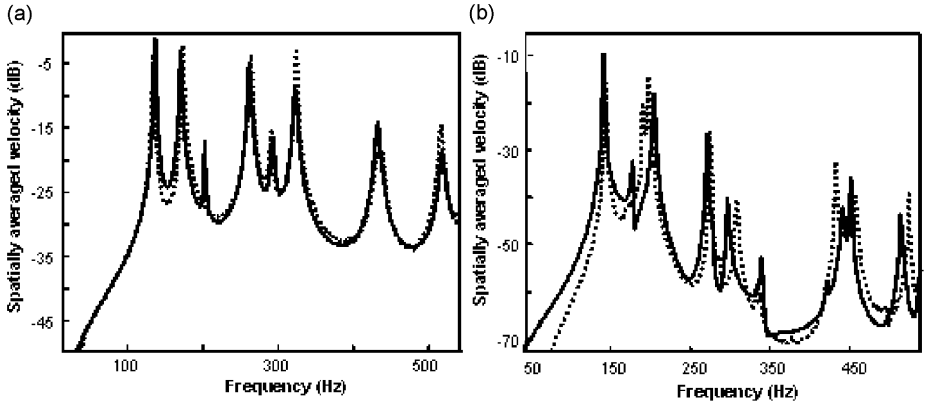

Fig. 5. Experimental validation of (a) the fuselage and (b) the trim panel of a double panel system measured at 25 points. A unit point force was applied at a non center position on the fuselage panel. Theory (——). Experiment (------).

The comparison shows a good match across the frequency range of interest (50–500 Hz) and should be sufficiently accurate to capture all of the important physics concerned with sound transmission through the double panel system. As expected, exact matching between model and experiment becomes difficult as the system complexity increases. The discrepancies at low frequencies are a result of minor frame motions which cause a zero in the measured response at around 40 Hz. The frame in the model is assumed to be rigid but the experimental frame, although heavy, was not perfectly attached to ground.

3.2. Experimental validation for double panel system with sandwiched HG blanket

This section presents the experimental validation for a double panel system embedded with three different HG-blankets. The first HG-blanket (HG blanket #1) has one mass (23 g) inserted inside the poro-elastic media, placed in the center of the plate, near the surface of the poro-elastic media to target the 1–1 mode. This is shown in Fig. 6(a).

Fig. 6(b) shows the mass positions of the two mass inclusions, 17 and 6 g, inside HG blanket #2. The first mass (17 g) is placed in the center of the plate, near the surface of the poro-elastic media to target the 1–1 mode. Its mass is approximately 74% of the total mass (23 g) added to the poro-elastic material, due to the fact that the fundamental frequency is very low and the resonant frequency decreases with increasing the weight of the mass inclusion. The mass was placed in the center because the anti-node of the 1–1 mode is in the center of the plate. A 6 g mass was positioned at an off center position at $x/L_x = 0.3$ and $y/L_y = 0.7$ to target the 2–1 mode, following a similar physical principle as discussed above: the second resonant frequency of the fuselage panel is higher than the fundamental frequency. Hence, the resonant frequency of the mass inclusion is tuned to a higher frequency by decreasing its weight and depth inside the porous layer. An example of the resonant frequency of the mass inclusion increasing with decreasing the depth of the mass inclusion is shown by Kidner et al. [36]. Consideration was also given to the interaction of the second mass inclusion with the 1–2 and 2–2 modes and thus the inclusion was not placed exactly on the anti-node of the 2–1 but slightly off so that the mass could also interact with the 1–2 and 2–2 modes.

HG blanket #3 was constructed to target the 1–1 mode with the heavy mass at the position $x/L_x = 0.7$ and $y/L_y = 0.5$. In addition, a second mass was placed at the position $x/L_x = 0.3$ and $y/L_y = 0.5$ as shown in Fig. 6(b) to target the 1–3 mode of the fuselage panel.

Details of how the embedded masses are tuned are presented in detail in Ref. [17]. The total weight of the embedded masses of all HG blankets presented in this paper is approximately 10% of the fuselage panel weight. Other than the inclusion of the HG blankets, the experimental setup used for the experimental validation of the double panel system is identical with the one used in this section. Due to the addition of the HG blanket the cavity thickness is reduced due to the fact that the distance between fuselage and trim is kept constant. Table 2 presents the HG blanket properties as well as the modified cavity parameters for the experimental validation of the double panel system with HG blanket inside. The fuselage and trim parameters are shown on the previous section in Table 1.

Fig. 7 shows the comparison of predicted (a) and measured (b) spatially averaged velocity of the double panel system fuselage panel with and without sandwiched HG blanket #1. HG blanket #1 was designed to target the 1–1 mode of the fuselage at approximately 130 Hz. A unit point force was applied at a non-center position, as shown in Fig. 3, at the fuselage panel to excite all plate modes. Theory and experiment show the same trends: the mode split around 130 Hz caused a significant drop in the vibration response.

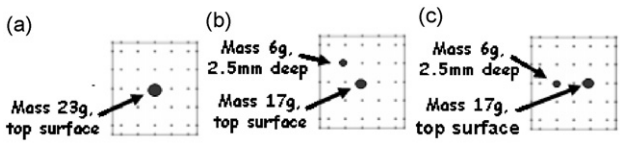

Fig. 6. Mass positions of: (a) HG blanket #1, (b) HG blanket #2 and (c) HG blanket #3 used in the experimental validation of the design tool.

Table 2
Model parameters of HG blanket and cavity.

Parameter	Value	Units
Material properties of the HG blanket		
Length	0.298	m
Width	0.198	m
Thickness	0.05	m
Density	50	kg/m^3
Modulus of elasticity	2.2×10^5	N/m^2
Poisson's ratio	0.3	–
Tortuosity	1.7	–
Flow resistivity	3.2×10^4	$N\,s/m^4$
Porosity	0.95	–
Atmospheric pressure	1.0325×10^5	N/m^2
Structural damping	0.0001	–
Viscous characteristic length	5×10^{-5}	–
Thermal characteristic length	1.1×10^{-4}	–
Total weight of embedded masses	23	g
Material properties of the cavity		
Thickness	0.05	m
Density	1.2	kg/m^3
Speed of sound	343	m/s
Damping	0.01	–

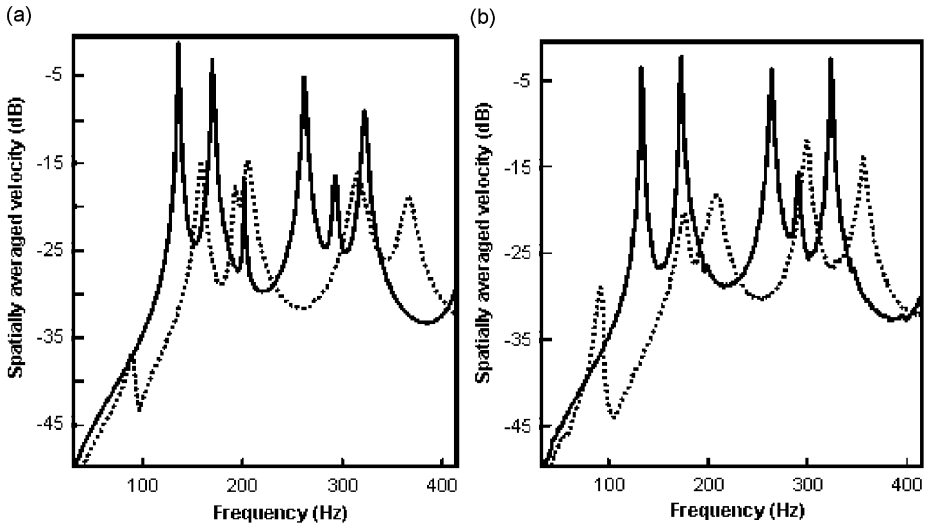

Fig. 7. Comparison of spatially averaged velocity of a fuselage panel inside a double panel system with and without sandwiched HG blanket #1: (a) predicted response and (b) measured response. Without treatment (——). With HG blanket treatment (------).

Fig. 8 shows the comparison of predicted (a) and measured (b) spatially averaged velocity of the double panel system trim panel with and without sandwiched HG blanket. One can see that the mode split of the first fuselage mode around 130 Hz in Fig. 7 caused by the HG blanket, also resulted in a mode split for the first mode of the trim panel, since the fuselage and trim panels are highly coupled by the air cavity at this frequency. Hence, a drop in the vibration response of the fuselage caused a drop in vibration response of the

trim. It can be seen in Fig. 8 that the drop in the vibration response due to the mode split at around 130 Hz is quite significant.

Fig. 9 shows a comparison of the calculated sound power radiated from the trim panel of the double panel system with sandwiched HG blanket using measured and calculated trim velocities. Plotted are the spectral density on the left and one-third octave band on the right. The results of the experimental validation in the frequency range of interest show that the dynamics of the fuselage are captured. The results match up well at lower frequencies by duplicating the physics of the 1–1 mode split on the fuselage. The damping levels do not match perfectly at the modes but the overall dB level is well matched. A significant level of complexity has been added to the analytical model between the double panel system with and without the HG blanket. The one-third octave band plot verifies once again that the theoretical model captures the basic physics of the system studied.

In order to validate the mathematical model of the double panel system with HG blankets #2 and #3 to compare it to the porous media case (HG blanket without mass inclusions), the predicted spatially averaged velocity of the trim panel was plotted over the frequency of interest (50–500 Hz) as shown in Fig. 10. The response of the double panel system with porous media is a reference showing the effectiveness of the designed HG blanket. The HG blanket #2 targeted the first mode of the trim panel with the large mass. Due to the mode split of the 1–1 mode, the HG blanket #2 lowers the vibration response up to 160 Hz by a significant amount. The second mass inside HG blanket #2 has no effect on the trim side. This is due to the fact that the

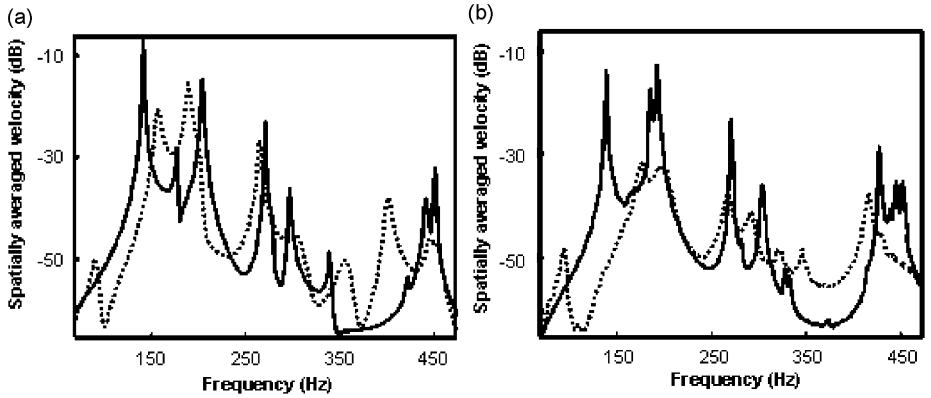

Fig. 8. Comparison of spatially averaged velocity of a trim panel inside a double panel system with and without sandwiched HG blanket #1: (a) predicted response and (b) measured response. Without treatment (——). With HG blanket treatment (------).

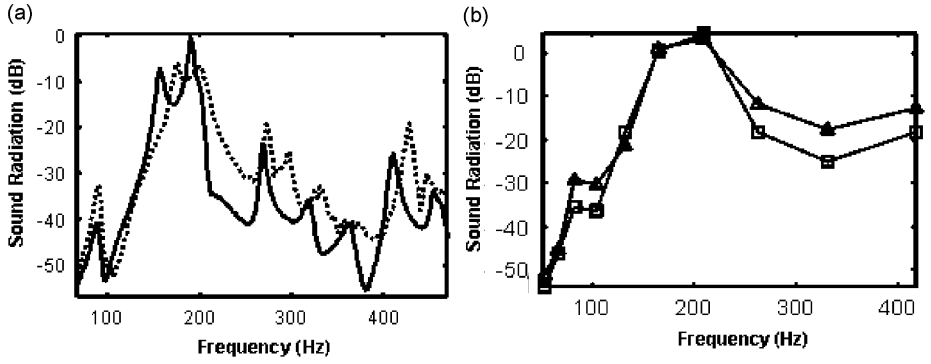

Fig. 9. Comparison of experimental and predicted radiated sound power of the trim side of a double panel system with sandwiched HG blanket #1. (a) presents the spectral density. Theory (——). Experiment (------). (b) is a one-third octave band plot. Theory (—□—). Experiment (—△—). HG blanket is designed to target the 1-1 mode of the fuselage pane. A unit point force was applied at a non center position on the fuselage panel.

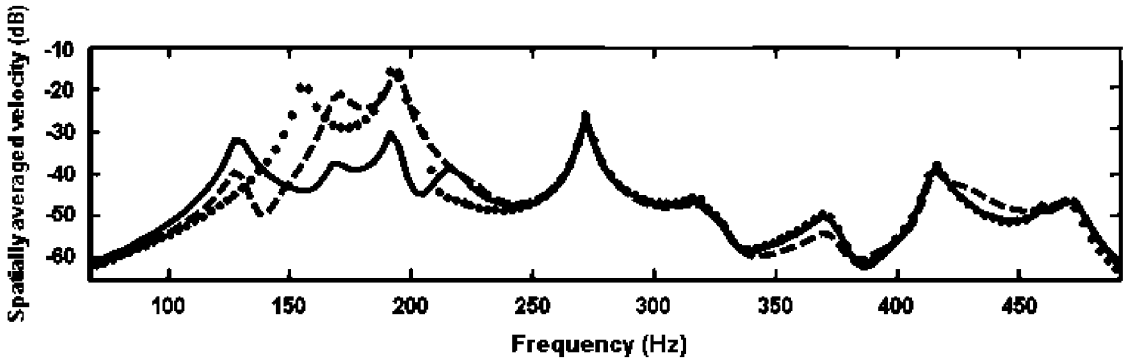

Fig. 10. Predicted response of a double panel system. Plotted is the spatially averaged velocity of the trim panel with acoustic blanket glued on top and an HG blanket glued on top of the fuselage panel. Poro-elastic layer (****). HG blanket #2 (-----). HG blanket #3 (——).

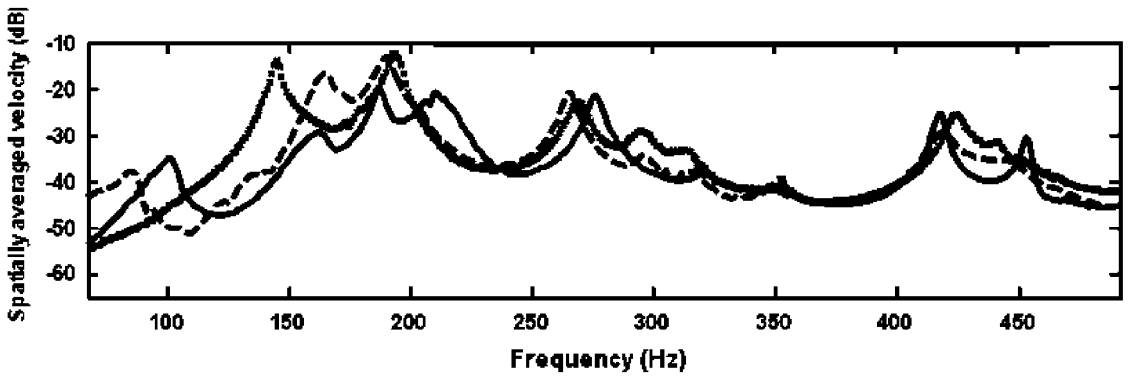

Fig. 11. Measured response of a double panel system: spatially averaged velocity of the trim panel with either acoustic blanket or HG blanket glued on top of the fuselage panel. Poro-elastic layer (****). HG blanket #2 (-----). HG blanket #3 (——).

coupling between the modes of the two panels varies from mode to mode. Thus, only certain modes of the fuselage panel couple strongly to the trim panel. The 1–2 mode is not an efficient radiator, thus targeting the 1–2 mode on the fuselage panel does not reduce significantly the vibration response of the trim panel. HG blanket #3 achieves broad control over the 140–220 Hz range where the first two modes dominate. Both HG blankets and the poro-elastic layer without mass inclusions have similar performances above 250 Hz. It should be noted that the modes described here represent the coupled modes of the double panel system. It should also be noted that the attenuation achieved can be due to controlling resonances **or** altering the mode shapes of the fuselage panel in order to reduce coupling across the cavity.

Fig. 11 shows the corresponding measurements to Fig. 10. Although the mode splits occur in the experiments at lower frequencies than in the predictions, the relative characteristics of both results are similar. The experimental result for the HG blanket #2 shows that the first mode split was more significant than the second mode split, whereas the theoretical model shows equal significance for both mode splits.

In summary, the above results show that an effective analytical model has been developed and verified. The results presented using HG blankets to target certain modes of the fuselage also show the potential of the HG blanket to reduce the interior noise levels of an aircraft in the low frequency region, i.e. below 500 Hz.

4. Conclusions

This paper has presented an experimental validation of a numerical model predicting the response of a double panel system with sandwiched HG blanket and air cavity inside. An impedance and mobility method

approach was used to couple the analytical solutions of the fuselage and trim panel and air cavity with the finite element model of the HG blanket.

The experimental and numerical results presented indicate that the analytical model correctly predicts the experimental response of the double panel system with HG blankets, and can be used as a design tool. It was also shown that it is possible to target certain modes of the fuselage panel in a double panel system by tuning the masses inside the HG blanket to the resonant frequencies of the fuselage panel. This results in the reduction of the vibration levels of the fuselage which can lead to the reduction of the vibration of the trim and in turn lead to reductions in sound radiation. However, strictly speaking, reduction in sound radiation is only possible if the amplitudes of the efficiently radiating modes (or "radiation modes" [27]) of the trim are reduced. Although the efficiently coupled fuselage modes are likely to dominate the transfer of energy to the trim the coupling of the fuselage and the trim panel through the cavity is complicated and the authors suggest the use of optimizations routines to design an efficient HG blanket. The HG blanket still performs well at frequencies above 500 Hz [37] due to the presence of the acoustic foam. Overall, the HG blanket has shown potential for providing good noise reduction over a wide frequency bandwidth.

Acknowledgments

This project was supported by SMD Corp. under a NASA SBIR Grant A2.04-9836. In particular the support and collaboration of Prof. Rob Clark, Dr. Curtis Mitchell, Dr. Mike Kidner, Prof. Paolo Gardonio, Prof. Chris Fuller, Dr. Ralf Gramlich, Daniel Theurich, Andreas Wagner, David Bartylla, Parham Shahidi and Rachel Scott is gratefully acknowledged.

Appendix A. Impedance and mobility matrix expressions for porous media

The basic equations for the poro-elastic model where presented by Allard [38] and further developed for the HG blanket by Gautam et al. [39]. The basic equation of the finite element model is defined such as

$$\mathbf{f} = \mathbf{G}_{Poro}\mathbf{x}, \tag{A.1}$$

where $\mathbf{f}$ and $\mathbf{x}$ are column vectors of the applied nodal forces and the nodal displacements, respectively. $\mathbf{G}_{Poro}$ is derived from the equation of motion for the poro-elastic medium

$$\mathbf{G}_{Poro}(\omega) = -\omega^2\mathbf{M}_P + j\omega\mathbf{C}_P(\omega) + \mathbf{K}_P(\omega). \tag{A.2}$$

$\mathbf{M}_P$, $\mathbf{C}_P$ and $\mathbf{K}_P$ are the equivalent "mass", "damping" and "stiffness" matrices and ω is the circular frequency. In order to get the relationship between force and velocity at the boundary condition nodes (base and top nodes) and the nodes in between, (A.1) can be written as

$$\begin{Bmatrix} \mathbf{f}_{NBC} \\ \mathbf{f}_{BC} \end{Bmatrix} = \begin{bmatrix} \mathbf{G}_{11} & \mathbf{G}_{12} \\ \mathbf{G}_{21} & \mathbf{G}_{22} \end{bmatrix} \begin{Bmatrix} \mathbf{x}_{NBC} \\ \mathbf{x}_{BC} \end{Bmatrix}, \tag{A.3}$$

with

$$\mathbf{f}_{BC} = \begin{Bmatrix} \mathbf{f}_{BC_{\mathrm{Bs}}} \\ \mathbf{f}_{BC_{\mathrm{Bf}}} \\ \mathbf{f}_{BC_{\mathrm{Ts}}} \\ \mathbf{f}_{BC_{\mathrm{Tf}}} \end{Bmatrix}, \quad \mathbf{f}_{NBC} = \begin{Bmatrix} \mathbf{f}_{NBC_{\mathrm{S}}} \\ \mathbf{f}_{NBC_{\mathrm{f}}} \end{Bmatrix}, \quad \mathbf{x}_{BC} = \begin{Bmatrix} \mathbf{x}_{BC_{\mathrm{Bs}}} \\ \mathbf{x}_{BC_{\mathrm{Bf}}} \\ \mathbf{x}_{BC_{\mathrm{Ts}}} \\ \mathbf{x}_{BC_{\mathrm{Tf}}} \end{Bmatrix}, \quad \mathbf{x}_{NBC} = \begin{Bmatrix} \mathbf{x}_{NBC_{\mathrm{S}}} \\ \mathbf{x}_{NBC_{\mathrm{f}}} \end{Bmatrix},$$

where for the force $\mathbf{f}_{BC}$ the first indexes "BC" and "NBC" stand for the boundary condition and non-boundary condition nodes, respectively, and the second indexes "Bs", "Bf", "Ts" and "Tf" stand for the bottom nodes solid phase/fluid phase and the top nodes solid phase/fluid phase, respectively. The force and displacement relationship of the nodes with fixed boundary conditions are obtained by setting the external force at the non-boundary condition nodes to zero ($\mathbf{f}_{NBC} = 0$):

$$\mathbf{f}_{BC} = (\mathbf{G}_{22} - \mathbf{G}_{21}\mathbf{G}_{11}^{-1}\mathbf{G}_{12})\mathbf{x}_{BC}. \tag{A.4}$$

However, since $\mathbf{v}_{BC} = j\omega\mathbf{x}_{BC}$, the impedance at the boundary is given by

$$\mathbf{Z} = \frac{1}{j\omega}(\mathbf{G}_{22} - \mathbf{G}_{21}\mathbf{G}_{11}^{-1}\mathbf{G}_{12}) \tag{A.5}$$

and the mobility matrix is the inverse of the impedance matrix:

$$\mathbf{M} = \mathbf{Z}^{-1}. \tag{A.6}$$

One can now split up the impedance or mobility matrix in a solid–solid phase, solid–fluid phase, fluid–solid phase and fluid–fluid phase seeing how half of the rows in the impedance or mobility matrix are due to the fluid phase and the other half due to the solid phase of the poro-elastic material. The impedance and mobility matrix can then be split up into:

$$\mathbf{Z} = \begin{bmatrix} \mathbf{Z}_{ss} & \mathbf{Z}_{sf} \\ \mathbf{Z}_{fs} & \mathbf{Z}_{ff} \end{bmatrix} \quad \text{and} \quad \mathbf{M} = \begin{bmatrix} \mathbf{M}_{ss} & \mathbf{M}_{sf} \\ \mathbf{M}_{fs} & \mathbf{M}_{ff} \end{bmatrix},$$

with

$$\mathbf{Z}_{ss} = \begin{bmatrix} \mathbf{Z}_{Bss} \\ \mathbf{Z}_{Tss} \end{bmatrix}, \quad \mathbf{Z}_{sf} = \begin{bmatrix} \mathbf{Z}_{Bsf} \\ \mathbf{Z}_{Tsf} \end{bmatrix}, \quad \mathbf{Z}_{fs} = \begin{bmatrix} \mathbf{Z}_{Bfs} \\ \mathbf{Z}_{Tfs} \end{bmatrix}, \quad \mathbf{Z}_{ff} = \begin{bmatrix} \mathbf{Z}_{Bff} \\ \mathbf{Z}_{Tff} \end{bmatrix},$$

and

$$\mathbf{Z}_{ss} = \begin{bmatrix} \mathbf{Z}_{Bss} \\ \mathbf{Z}_{Tss} \end{bmatrix}, \quad \mathbf{Z}_{sf} = \begin{bmatrix} \mathbf{Z}_{Bsf} \\ \mathbf{Z}_{Tsf} \end{bmatrix}, \quad \mathbf{Z}_{fs} = \begin{bmatrix} \mathbf{Z}_{Bfs} \\ \mathbf{Z}_{Tfs} \end{bmatrix}, \quad \mathbf{Z}_{ff} = \begin{bmatrix} \mathbf{Z}_{Bff} \\ \mathbf{Z}_{Tff} \end{bmatrix},$$

where the indexes "B" and "T" represent the bottom and top nodes, respectively. The stress and strain relationship for a porous material can be written as

$$\boldsymbol{\sigma}_s = \mathbf{D}_s\boldsymbol{\varepsilon}_f + \mathbf{D}_{sf}\boldsymbol{\varepsilon}_f, \tag{A.7}$$

$$\boldsymbol{\sigma}_f = \mathbf{D}_{fs}\varepsilon_s + \mathbf{D}_{fs}\varepsilon_s = h\mathbf{p}. \tag{A.8}$$

The solid phase stress and strain are the force per unit area and the spatial gradient of the solid phase displacement. The fluid phase stress is the pressure and the fluid phase strain is the volumetric strain, or the divergence of the volume displacement. The total stress on a boundary is the summation of the solid phase and fluid phase stress

$$\boldsymbol{\sigma} = \boldsymbol{\sigma}_s + \boldsymbol{\sigma}_f. \tag{A.9}$$

The effective displacement of the boundary depends on if it is a fluid phase or solid boundary. Consider a very thin layer of fluid phase just in front of the porous material. The effective velocity at the boundary is $(1–h)\mathbf{v}_s + h\mathbf{v}_f$. In this case the relationship between the force acting on the fluid phase and the total velocity at the boundary is given with the mobility matrix $\mathbf{M}_f$ such that

$$\mathbf{M}_f\mathbf{f}_f = (1-h)\mathbf{v}_s + h\mathbf{v}_f. \tag{A.10}$$

Consider an infinitesimally thin structural boundary, such that the fluid phase and solid phase velocities are the same. Therefore in this case the relationship between the force acting on the porous material and the velocity of the solid phase at the boundary is given with the mobility matrix $\mathbf{M}_s$ such that

$$\mathbf{v}_s = \mathbf{M}_s(\mathbf{f}_s + \mathbf{f}_f). \tag{A.11}$$

The relationship between the solid phase and fluid phase velocities and forces in the finite element model are

$$\mathbf{v}_s = \mathbf{M}_{sf}\mathbf{f}_f + \mathbf{M}_{ss}\mathbf{f}_s, \tag{A.12}$$

$$\mathbf{v}_f = \mathbf{M}_{ff}\mathbf{f}_f + \mathbf{M}_{fs}\mathbf{f}_s, \tag{A.13}$$

$$\mathbf{f}_s = \mathbf{Z}_{sf}\mathbf{v}_f + \mathbf{Z}_{ss}\mathbf{v}_s, \tag{A.14}$$

$$\mathbf{f}_f = \mathbf{Z}_{ff}\mathbf{v}_f + \mathbf{Z}_{fs}\mathbf{v}_s. \tag{A.15}$$

The total force $\mathbf{f}$ applied on the porous material is split into a force applied on the solid phase $\mathbf{f}_s$ and on the fluid phase $\mathbf{f}_f$, therefore it is assumed that

$$\mathbf{f}_s = (1-h)\mathbf{f} \quad \text{and} \quad \mathbf{f}_f = h\mathbf{f}. \tag{A.16}$$

Hence

$$\mathbf{v}_s = \left(\mathbf{M}_{sf} + \frac{1-h}{h}\mathbf{M}_{ss}\right)\mathbf{f}_f, \tag{A.17}$$

$$\mathbf{v}_f = \left(\mathbf{M}_{ff} + \frac{1-h}{h}\mathbf{M}_{fs}\right)\mathbf{f}_f. \tag{A.18}$$

Using the above equations, the mobility and impedance matrices of a porous material in contact with an air cavity can be expressed as

$$\mathbf{M}_f = h\mathbf{M}_{ff} + (1-h)(\mathbf{M}_{fs} + \mathbf{M}_{sf}) + \frac{(1-h)^2}{h}\mathbf{M}_{ss}, \tag{A.19}$$

$$\mathbf{Z}_f = \left(h\mathbf{M}_{ff} + (1-h)(\mathbf{M}_{fs} + \mathbf{M}_{sf}) + \frac{(1-h)^2}{h}\mathbf{M}_{ss}\right)^{-1}. \tag{A.20}$$

When calculating the solid phase impedance and mobility matrices, the solid phase velocity $\mathbf{v}_s$ and the fluid phase velocity $\mathbf{v}_f$ are equal:

$$\mathbf{v} = \mathbf{v}_s = \mathbf{v}_f. \tag{A.21}$$

Hence,

$$\mathbf{f}_s = (\mathbf{Z}_{sf} + \mathbf{Z}_{ss})\mathbf{v}_s, \tag{A.22}$$

$$\mathbf{f}_f = (\mathbf{Z}_{ff} + \mathbf{Z}_{fs})\mathbf{v}_s. \tag{A.23}$$

The mobility and impedance matrices of a porous material in contact with an elastic structure can be expressed such as

$$\mathbf{Z}_s = \mathbf{Z}_{sf} + \mathbf{Z}_{ss} + \mathbf{Z}_{ff} + \mathbf{Z}_{fs}, \tag{A.24}$$

$$\mathbf{M}_s = (\mathbf{Z}_{sf} + \mathbf{Z}_{ss} + \mathbf{Z}_{ff} + \mathbf{Z}_{fs})^{-1}. \tag{A.25}$$

The given impedance and mobility matrices in Eqs. (A.19),(A.20),(A.24) and (A.25) can be used to describe the HG blanket used in the impedance and mobility method depending on the boundary conditions.

Appendix B. Mobility matrix of single panel modeled with lumped mass on top

The measurements of the fuselage and trim panel are both measured with a 4 g accelerometer placed at an off center position $x/L_x = 0.1$and $y/L_y = 0.7$ as shown in Fig. 3. The accelerometer was modeled as a lumped mass and coupled to the plate in order to build a more rigorous mobility matrix for the plate. Fig. B.1 shows the free body diagram of a plate with and without taking the mass of the accelerometer m into account.

The equations for the plate modeled with a lumped mass on top of it with an input force $\mathbf{f}_A$ and output velocity $\mathbf{v}_A$, where the force due to the mass m is $\mathbf{f}_M$ and the velocity of the mass m at the mass location is $\mathbf{v}_M$, solved for $\mathbf{v}_A$, is given by

$$\mathbf{v}_M = \mathbf{M}_0\mathbf{f}_M = \mathbf{M}_{MA}\mathbf{f}_A - \mathbf{M}_{MM}\mathbf{f}_M,$$

$$\rightarrow \mathbf{f}_M = (\mathbf{M}_0 + \mathbf{M}_{MM})^{-1}\mathbf{M}_{MA}\mathbf{f}_A, \tag{B.1}$$

$$\mathbf{v}_A = \mathbf{M}_{AA}\mathbf{f}_A - \mathbf{M}_{AM}\mathbf{f}_M = (\mathbf{M}_{AA} - \mathbf{M}_{AM}(\mathbf{M}_0 + \mathbf{M}_{MM})^{-1}\mathbf{M}_{MA})\mathbf{f}_A. \tag{B.2}$$

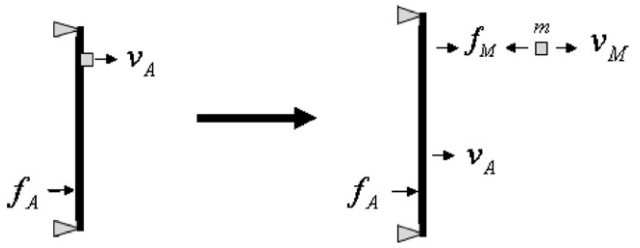

Fig. B.1. The free body diagram of a plate with and without taking the mass m of the accelerometer into account.

$\mathbf{M}_0$ is the mobility of the mass m, $\mathbf{M}_{AA}$, $\mathbf{M}_{AM}$, $\mathbf{M}_{MA}$, and $\mathbf{M}_{MM}$ are input and transfer plate mobility matrices with respect to the plate locations (index "A") and mass locations (index "M"). The output velocity $\mathbf{v}_A$ in Eq. (B.2) which describes the velocity at all locations on the plate, is expressed as an augmented mobility matrix $\mathbf{M}_{\text{equivalent}}$ times the input force where

$$\mathbf{M}_{\text{equivalent}} = \mathbf{M}_{AA} - \mathbf{M}_{AM}(\mathbf{M}_0 + \mathbf{M}_{MM})^{-1}\mathbf{M}_{MA}. \tag{B.3}$$

$\mathbf{M}_{\text{equivalent}}$ equivalent was used modeling both, the fuselage and the trim and the result was a higher accuracy for the experimental validation part of the project, not only on higher, but also at low frequencies (below 400 Hz), where the additional lumped mass of the accelerometer would result in an asymmetry of the plate and would let the uneven modes become more dominant when computing the double panel system.

References

[1] J.F. Wilby, Aircraft interior noise, *Journal of Sound and Vibration* 190 (1996) 545–564.
[2] J.P. Carneal, Active Structural Acoustic Control of Double Panel Systems Including Hierarchical Control Approaches, Ph.D. Thesis, Virginia Polytechnic Institute and State University, 1996.
[3] P. Gardonio, S.J. Elliott, Active control of structure-borne and airborne sound transmission through double panel, *Journal of Aircraft* 36 (1999) 1023–1032.
[4] P.A. Nelson, S.J. Elliott, *Active Control of Sound*, Academic Press, London, 1993.
[5] C.R. Fuller, Active control of sound transmission/radiation from elastic plates by vibration inputs. I—analysis, *Journal of Sound and Vibration* 136 (1990) 1–15.
[6] S.J. Elliott, P.A. Nelson, I.M. Stothers, C.C. Boucher, Preliminary results of in-flight experiments on the active control of propeller-induced cabin noise, *Journal of Sound and Vibration* 128 (1989) 355–357.
[7] S.J. Elliott, P.A. Nelson, I.M. Stothers, C.C. Boucher, In-flight experiments on the active control of propeller-induced cabin noise, *Journal of Sound and Vibration* 140 (1990) 219–238.
[8] K.E. Heitman, J.S. Mixson, Laboratory study of cabin acoustic treatments installed in an aircraft fuselage, *Journal of Aircraft* 23 (1986) 32–38.
[9] J.S. Mixson, L.A. Roussos, C.K. Barton, R. Vaicaitis, M. Slazak, Laboratory study of add-on treatments for interior noise control in light aircraft, *Journal of Aircraft* 20 (1983) 516–522.
[10] W.V. Bhat, J.F. Wilby, Interior noise radiated by an airplane fuselage subjected to turbulent boundary layer excitation and evaluation of noise reduction treatments, *Journal of Sound and Vibration* 17 (1971) 466–472.
[11] G. SenGupta, Reduction of low frequency cabin noise during cruise condition by stringer and frame damping, *American Institute of Aeronautics and Astronautics Journal* 17 (1979) 229–236.
[12] C.I. Holmer, Approach to interior noise control, part I: damped trim panels, *Journal of Aircraft* 22 (1985) 618–623.
[13] H. Baumgartl, Lightweight, versatile all-rounder, *Kunststoffe International* 96 (2006) 78–82.
[14] S.J. Estève, M.E. Johnson, Reduction of sound transmission into a circular cylindrical shell using distribute vibration absorbers and Helmholtz resonators, *Journal of the Acoustical Society of America* 112 (2002) 2840–2848.
[15] H. Osman, M.E. Johnson, C.R. Fuller, P. Marcotte, Interior noise reduction of composite cylinders using distributed vibration absorbers, *Proceedings of the Seventh AIAA/CEAS Aeroacoustics Conference*, Vol. 2, AIAA 2001-2230, Maastricht, The Netherlands, 2001, Collection of Technical Papers, A01-30800 07-71.
[16] M.R.F. Kidner, C.R. Fuller, B. Gardner, Increase in transmission loss of single panels by addition of mass inclusions to a poro-ealstic layer: experimental investigation, *Journal of Sound and Vibration* 294 (2006) 466–472.
[17] F. Sgard, N. Atalla, C.K. Amedin, Vibro-acoustic behavior of a cavity backed by a plate coated with a meso-heterogeneous porous material, *Acta Acoustica United with Acoustica* 93 (2007) 106–114.
[18] N. Atalla, C.K. Amedin, F. Sgard, Numerical and experimental investigation of the vibro-acoustics of a plate backed cavity coated with a heterogeneous porous material, SAE Meeting, Traverse City, USA, 2003-01-1453, 2003.

[19] K. Idrisi, M.E. Johnson, J.P. Carneal, M.R.F. Kidner, Passive control of sound transmission through a double panel system using heterogeneous (HG) blankets, Part II: HG parametric studies, *Proceedings of Noise-Con '07*, Reno, Nevada, 2007.
[20] W.T. Thomson, *Vibration Theory and Applications*, Prentice-Hall Inc., Englewood Cliffs, NJ, 1965.
[21] J. Ormondroyd, J.P. Den Hartog, Theory of the Dynamic Vibration Absorber, *Transactions of ASME* 50 (1928) 9–22.
[22] J.P. Den Hartog, *Mechanical Vibrations*, Dover Publications, McGraw Hill, New York, 1934.
[23] P. Gardonio, M.J. Brennan, Active isolation of structural vibration on a multiple-degree-of-freedom system. Part I: the dynamics of the system, *Journal of Sound and Vibration* 207 (1997) 61–93.
[24] G. Warburton, The vibration of rectangular plates, *Proceedings of the Institution of Mechanical Engineers*, Vol. 168, 1954, pp. 371–384.
[25] R. Panneton, N. Atalla, An efficient finite element scheme for solving the three-dimensional poroelastic problem in acoustics, *Journal of the Acoustical Society of America* 101 (1997) 3287–3298.
[26] L. Kinsler, A. Frey, A. Coppens, J. Sanders, *Fundamentals of Acoustics*, Wiley, New York, 1999.
[27] S.J. Elliott, M.E. Johnson, Radiation modes and the active control of sound power, *Journal of the Acoustical Society of America* 94 (1993) 2194–2204.
[28] M.R. Bai, M. Tsao, Estimation of sound power of baffled planar sources using radiation matrices, *Journal of the Acoustical Society of America* 112 (2002) 876–883.
[29] A.P. Berkhoff, Sensor scheme design for active structural acoustic control, *Journal of the Acoustical Society of America* 108 (2000) 1037–1045.
[30] F.A. Firestone, A new analogy between mechanical and electrical systems, *Journal of the Acoustical Society of America* 4 (1933) 249–267.
[31] P. Gardonio, M.J. Brennan, On the origin and development of mobility and impedance methods in structural dynamics, *Journal of Sound and Vibration* 249 (2002) 557–573.
[32] P. Gardonio, M.J. Brennan, *Mobility and Impedance Methods in Structural Dynamics*, Spon Press, New York, 2004.
[33] K.A. Mulholland, H.D. Parbrook, A. Cummings, The transmission loss of a double panel, *Journal of Sound and Vibration* 6 (1967) 324–334.
[34] K.R. Matthews, Elementary Linear Algebra, Department of Mathematics, University of Queensland, 1991: 〈http://www.numbertheory.org/book/〉, Accessed 21 February 6, 2008.
[35] A.W. Leissa, Vibration of Plates, NASA SP-160, 1969.
[36] M.R.F. Kidner, K. Idrisi, M.E. Johnson, J.P. Carneal, Comparison of experimental, finite element and wave based models for mass inclusions in poro-elastic layers, *Proceedings of ICSV* 14, Cairns, Australia, 2007, Paper 577: www1–www8.
[37] K. Idrisi, M.E. Johnson, J.P. Carneal, Passive control of sound transmission through a double panel system using heterogeneous (HG) blankets, Part III: HG design strategies, *Proceedings of Noise-Con '07*, Reno, Nevada, 2007.
[38] J.F. Allard, *Propagation of Sound in Porous Media, Modeling Sound Absorbing Materials*, Elsevier Science Publishers Ltd., London, 1993.
[39] A. Gautam, C.R. Fuller, J.P. Carneal, Application of the heterogeneous blankets (HG blankets) for controlling the base structure vibration levels, *Proceedings of Noise-Con `05*, Minneapolis, Minnesota, 2005.